# Silver Nanoparticles Induced RNA Polymerase-Silver Binding and RNA Transcription Inhibition in Erythroid Progenitor Cells

**Zhe Wang,[†] Sijin Liu,[†,*] Juan Ma,[†] Guangbo Qu,[†] Xiaoyan Wang,[†] Sujuan Yu,[†] Jiuyang He,[‡] Jingfu Liu,[†] Tian Xia,[§] and Gui-Bin Jiang[†]**

[†]State Key Laboratory of Environmental Chemistry and Ecotoxicology, Research Center for Eco-Environmental Sciences, Chinese Academy of Sciences, Beijing 100085, China, [‡]Department of Biomedical Engineering, Tufts University, Medford, Massachusetts 02155, United States, and [§]Division of NanoMedicine, Department of Medicine, University of California—Los Angeles, Los Angeles, California 90095, United States

**ABSTRACT** Due to its antimicrobial activity, nanosilver (nAg) has become the most widely used nanomaterial. Thus far, the mechanisms responsible for nAg-induced antimicrobial properties and nAg-mediated toxicity to organisms have not been clearly recognized. Silver (Ag) ions certainly play a crucial role, and the form of nanoparticles can change the dissolution rate, bioavailability, biodistribution, and cellular uptake of Ag. However, whether nAg exerts direct "particle-specific" effects has been under debate. Here we demonstrated that nAg exhibited a robust inhibition on RNA polymerase activity and overall RNA transcription through direct Ag binding to RNA polymerase, which is separated from the cytotoxicity pathway induced by Ag ions. nAg treatment *in vitro* resulted in reduced hemoglobin concentration in erythroid cells; *in vivo* administration of nAg in mice caused profound reduction of hemoglobin content in embryonic erythrocytes, associated with anemia in the embryos. Embryonic anemia and general proliferation deficit due to the significant inhibition on RNA synthesis, at least partially, accounted for embryonic developmental retardation upon nAg administration. To date, there is no conclusive answer to the sources of nAg-mediated toxicity: Ag ions or "particle-specific" effects, or both. We here demonstrated that both Ag ions and nAg particles simultaneously existed inside cells, demonstrating the "Trojan horse" effects of nAg particles in posing biological impacts on erythroid cells. Moreover, our results suggested that "particle-specific" effects could be the predominant mediator in eliciting biological influences on erythroid cells under relatively low concentrations of nAg exposure. The combined data highlighted the inhibitory effect of nAg on RNA polymerase activity through a direct reciprocal interaction.

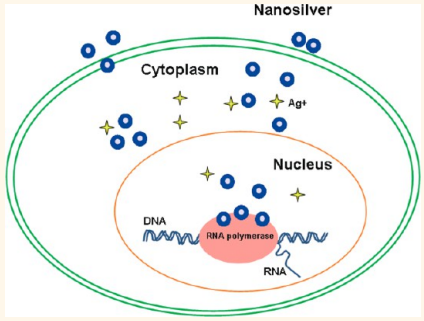


**KEYWORDS:** nanosilver · trojan horse · erythroid cells · RNA polymerase · transcription

With the explosive growth of nanotechnology, nanosilver (nAg) has become the most widely used nanomaterial.[1,2] Due to its novel properties, in particular, its intrinsic antimicrobial activity, nAg has been applied to diverse fields with significant advantages, such as medicine and personal care.[3−7] To date, the mechanisms underlying nAg-mediated antimicrobial activity have not been fully characterized. Meanwhile, large-scale applications of nAg-related products pose potential risks to the environment and health.[8,9] A number of studies have documented the toxicities of nAg in a variety of cells and organisms.[10−12] There is also possible interruption of genetic integrity,[13−15] because nAg could be readily taken up into cells and even the nuclei.[14,16] However, studies on nAg-mediated genotoxicity are still limited; thus far, there has been scarce investigation on the effect of nAg exposure on RNA polymerase activity and RNA polymerase-conducted transcription.

Until now, the sources of nAg-mediated toxicity have not been clearly determined and are without conclusive answer. In other words, the mechanism of nAg-mediated toxicity is not clear: ion effects, particle effects, or both. Previous studies have demonstrated that nAg has the potential to release Ag ions, and Ag ions could surely exert significant toxicity to cells and organisms.[3,17,18] However, whether nAg conducts

* Address correspondence to sjliu@rcees.ac.cn.

Received for review February 4, 2013 and accepted April 9, 2013.

**Published online April 09, 2013**
**10.1021/nn400594s**

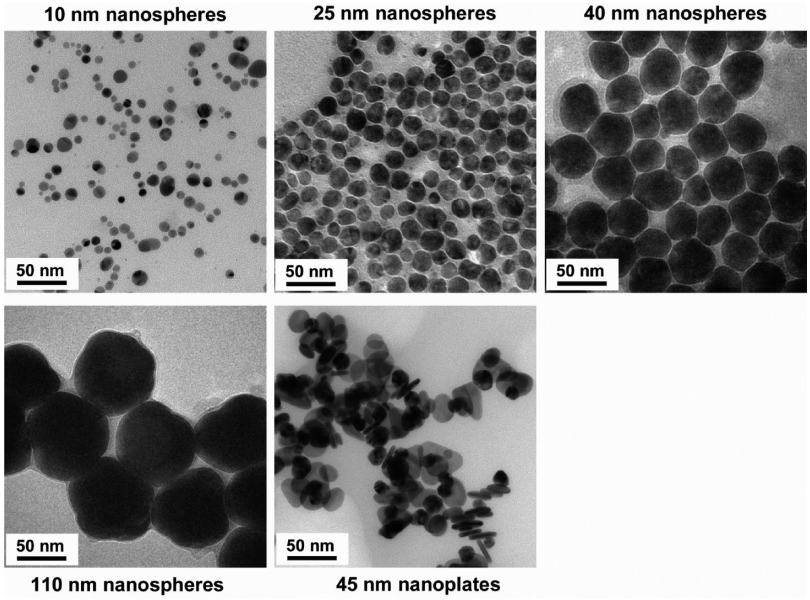


**Figure 1. Representative TEM images of nAg used in the current study. The scale was 50 nm and the original magnification was ×400000.**

direct particle effects has been in issue. In the current report, we employed a panel of nAg of different sizes and shapes, and their detailed properties are described in Table S1, with the representative TEM images shown in Figure 1. We studied the mechanisms responsible for nAg-induced cytotoxicity from the perspective of nAg's interference on RNA polymerase activity and the interaction between Ag and RNA polymerase in erythroid cells. We here chose erythroid cells because hemoglobins are the predominant proteins produced by these cells and, thus, it is relatively easy to study the regulation of mRNA transcription for globin genes. We demonstrated that nAg conduced a significant suppression on RNA polymerase activity and overall RNA transcription through direct Ag binding to RNA polymerase, and this effect was separated from the cytotoxicity pathway induced by Ag ions. Our results suggested that the particle effects could be the predominant mediator in inhibiting RNA transcription in erythroid cells under relatively low concentrations of nAg exposure. Our combined data confirmed the "Trojan horse" effects of nAg in exerting biological effects on erythroid cells.

## RESULTS AND DISCUSSION

We first surveyed the potential influence of nAg treatment on globin mRNA transcription by exposing mouse erythroleukemia (MEL) cells to nAg. MEL cells are erythroid progenitor cells at the stage of proerythroblast, and these cells continue to differentiate upon induction with DMSO.[19] As shown in Figure S1, the qRT-PCR analysis reflected a large reduction for both α-globin and β-globin mRNA concentrations in MEL cells treated with 10, 25, 40, or 110 nm spherical nAg, or 45 nm plate-like nAg, at a concentration of 1 μg/mL ($P < 0.001$), compared to those in control cells. It should be noted that all types of nAg used here caused no decrease in cell viability for MEL cells at 1 μg/mL (data not shown). Bioavailability of nanomaterials largely depends on their shape, size, and other properties such as surface charge. Regarding nAg, the particles could be readily taken up into cells through endocytosis,[14,16] and nAg particles in spherical shape have greater capability to cross the plasma membrane compared to other shapes. For example, a recent study by George et al. showed that Ag nanoplate had less cellular uptake by cells than spherical nAg particles.[20] In agreement with this finding, we observed greater inhibitory effect on α-globin and β-globin expression for nAg in spherical shape (i.e., 10, 25, 40, and 110 nm spherical nAg particles), compared to nAg in plate shape (Figure S1, $P < 0.05$). Furthermore, the size of nAg is also a crucial determinant for its bioavailability, and nAg particles with smaller size often revealed greater uptake by cells than those with larger size.[21] In the current study, among spherical nAg particles, nAg with the size of 10 or 25 nm showed greater inhibition on globin expression, especially for α-globlin (Figure S1, $P < 0.05$), than nAg with the size of 40 or 110 nm. Of 10 and 25 nm nAg, no significant difference was found in eliciting repression of globin mRNA levels (Figure S1, $P > 0.05$). Because small-size nAg (<10 nm) tends to have a greater rate of dissolution than large-size nAg (>10 nm),[18,20] we embarked on an investigation of the mechanisms underlying nAg-mediated inhibition on globin gene transcription by selecting 25 nm spherical nAg in the follow-up experiments.

To substantiate the above observations, we further assessed the levels of hemoglobin mRNAs in MEL cells

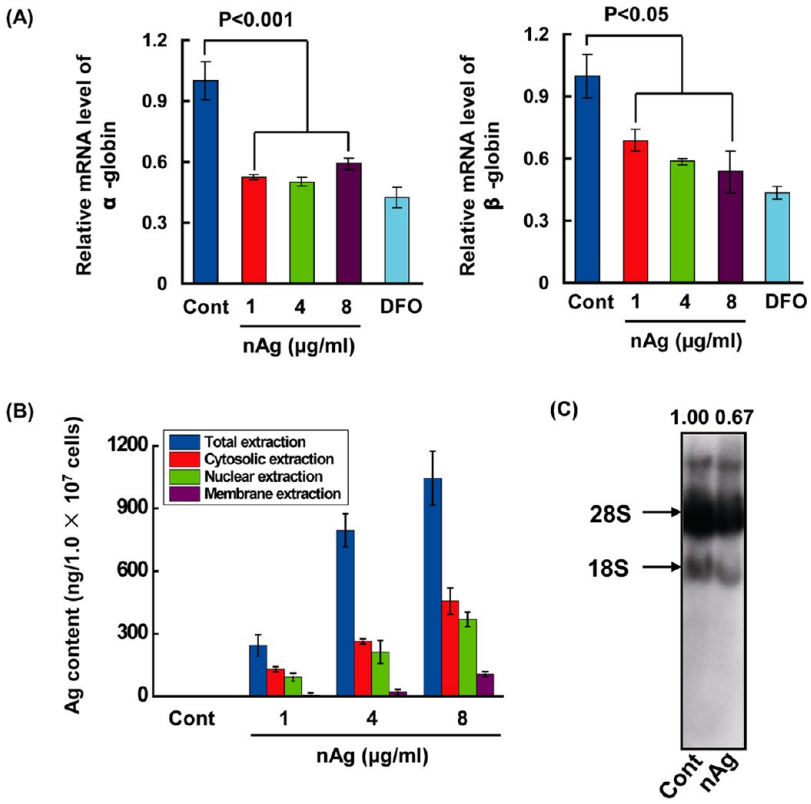


**Figure 2. Decreased RNA transcription upon nAg exposure. (A) Expression of globin mRNAs in erythroid cells. MEL cells were cultured with DMSO for 3 d and then exposed to nAg at various concentrations for an additional 3 d. DFO was used as a positive control at 4.6 $\mu$g/mL. The qRT-PCR analysis was performed with RNAs from these cells ($n$ = 4). (B) Quantitative distribution of nAg. MEL cells were similarly treated with nAg as described above. Total cell lysates and fractions of cytoplasm, nucleus and cell membrane were separated, digested and quantified for Ag content using the method of ICP-MS ($n$ = 4). (C) Autoradiogram of overall RNA synthesis. MEL cells were treated with 8 $\mu$g/mL nAg as described above. Total RNAs (20 $\mu$g) labeled with $^{32}$P were separated by agarose formaldehyde gel followed by autoradiography. The arrows indicate the positions of 28S and 18S rRNAs, respectively. The quantification of autoradiography for total RNAs was performed with the software Image J (NIH, U.S.A.), and the relative values are shown above the image.**

treated with 25 nm spherical nAg at 1, 4, and 8 $\mu$g/mL. As shown in Figure 2A, there was a significant decline in both $\alpha$-globin and $\beta$-globin mRNA levels at all concentrations of nAg treatment compared to the control ($P < 0.05$). We did not see a clear dose response for $\alpha$-globin in comparison to $\beta$-globin, and in fact, at 1 $\mu$g/mL it already reached the highest level of inhibition for $\alpha$-globin. The reason for this difference is likely that $\alpha$-globin is more sensitive to Ag treatment than $\beta$-globin, which needs further investigation in future studies. Our recent study demonstrated that iron is necessary for erythropoiesis and hemoglobin production, and iron deficiency leads to impaired erythroid differentiation and reduced hemoglobin content linked to microcytic anemia.[22] We used an iron chelator desferrioxamine (DFO) as a positive control to repress globin expression with about 50% reduction (Figure 2A, $P < 0.001$). To exclude the potential effect of nAg treatment on intracellular iron availability, we measured the intracellular liable iron pool (LIP) with FACS. As shown in Figure S2, the intracellular iron level reflected by the LIP value was not significantly affected in MEL cells upon exposure to nAg, compared to control cells, suggesting that nAg treatment elicited little effect on iron homeostasis in MEL cells. Thus, DFO could here serve as an ideal positive control, indicating repression of globin expression.

Biological effects of nanoparticles are closely related to their cellular transportation and intracellular localization. To understand the quantitative distribution of nAg inside cells, we then looked into Ag content in the whole cell lysates, and the fractions of cytoplasm, nucleus and cell membrane. Based on the ICP-MS results (Figure 2B), the total intracellular Ag content was approximately 1,000 ng per 1.0 $\times$ 10$^7$ MEL cells with exposure to 8 $\mu$g/mL nAg for 3 d, and the Ag mass greatly reduced with the decrease of nAg concentration to 4 and 1 $\mu$g/mL ($P < 0.05$). The Ag content in nuclear fraction accounted for >25% of the total intracellular Ag in the whole cell lysates from cells with the treatment of nAg (Figure 2B). The Ag content in cytoplasmic fraction was greater than that in nucleus, and nAg localized within plasma membrane was much less than that in cytoplasm or nucleus (Figure 2B, $P < 0.05$). These findings indicated that nAg could enter MEL cells and locate in cytoplasm and nucleus;

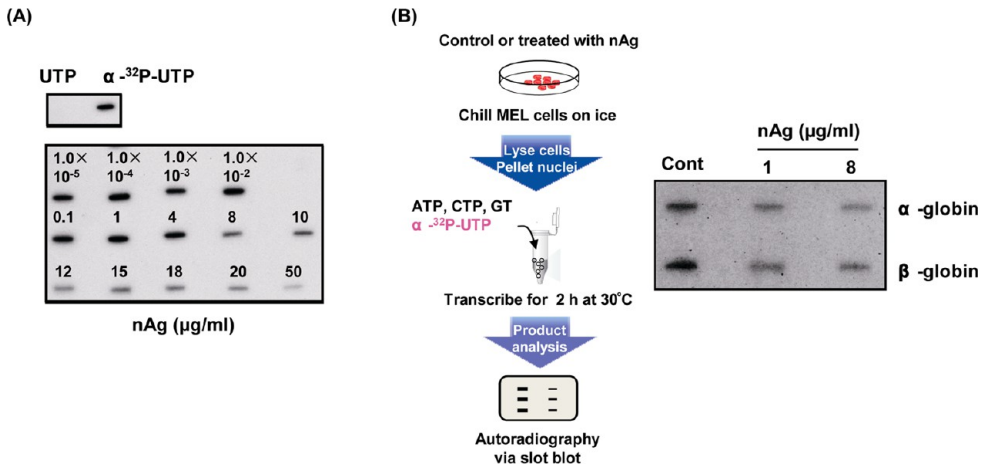


**Figure 3. Inhibition of RNA polymerase activity by nAg. (A) Autoradiogram of mRNA transcripts from the *in vitro* runoff experiments. RNAs with $^{32}$P labeling were extracted from runoff transcription systems, and were then used to hybridize with the plasmid DNA fragment on a membrane. The number above each band indicates the corresponding concentration of nAg used in the assays. (B) Autoradiogram of the nuclear run-on assay. The experimental schematic for nuclear run-on assay is shown on the left panel. MEL cells with or without nAg exposure were cultured for 4 d in the presence of DMSO. RNAs with $^{32}$P labeling were purified from the same number of nuclei and were then used for hybridization with globin cDNAs on a membrane.**

however, the form of Ag (nanoparticle or Ag ions) is unclear. Because there is a significant amount of Ag present in the nucleus, we hypothesized that the massive nuclear accumulation of Ag might interrupt the transcription machinery within the nucleus and, consequentially, impede RNA transcription. To validate this hypothesis, we assayed the overall efficacy of global RNA synthesis by labeling nascent RNAs with $^{32}$P in MEL cells with or without nAg treatment. The autoradiography of total RNAs extracted from MEL cells revealed that the overall synthesis of RNAs was hampered upon nAg exposure, as a large reduction of the intensity of total RNAs including 18S and 28S rRNAs from 8 $\mu$g/mL nAg-treated cells was observed compared to the control (>30% reduction, Figure 2C). These results together suggested that the accumulation of Ag in MEL cells substantially inhibited overall RNA transcription.

RNA polymerase (RNAP) is an enzyme that uses DNA as a template to produce RNA in the nucleus, and reduced polymerase activity leads to a decrease in RNA synthesis.[23] To determine whether the activity of RNA polymerase was affected by the presence of nAg, as manifested by the diminished globin mRNA concentrations in MEL cells described above, we evaluated the synthesis of nascent transcripts with autoradiography through an acellular runoff transcriptional assay. As shown in Figure 3A, the band intensity in the image of autoradiography was largely reduced in the presence of nAg in a dose-dependent manner. More than a 50% reduction of RNA synthesis was observed when the concentration of nAg reached 8 $\mu$g/mL (Figure 3A). Thereafter, a cellular nuclear run-on assay was performed in MEL cells to validate the results of the runoff assay (schematic shown in Figure 3B), where nuclear RNAs with $^{32}$P-labeling were isolated from control cells or cells treated with nAg, and hybridized to α-globin and $\beta$-globin cDNAs on a membrane. The synthesis of both α-globin and $\beta$-globin was reduced >2-fold in nAg-treated cells at 1 and 8 $\mu$g/mL (Figure 3B). These findings demonstrated that RNA polymerase-mediated transcription machinery was attenuated due to nAg treatment and nAg inhibited RNA polymerase-conducted transcriptional activity. However, these effects could be due to nAg particles or dissolved Ag ions.

Transformations of nanomaterials in biological environments would potentially change the rate of ion dissolution, behaviors, and even toxicological characteristics of nanomaterials.[24−26] We thus determined the size, zeta potential, and UV−visible spectrum of nAg in culture medium. We first characterized the size of nAg in ultrapure $H_2O$ at 8 $\mu$g/mL using a Zetasizer. An exclusive peak indicated that the hydrodynamic diameter of nAg was about 60 nm in $H_2O$ (Figure S3A). In order to find out whether proteins from FBS affected the hydrodynamic size of nAg, we assessed the hydrodynamic diameter of nAg at 8 $\mu$g/mL in medium with 10% FBS (a normal percentage for cell culture). As shown in Figure S3A, the hydrodynamic diameter of nAg in culture medium in the presence of 10% FBS kept similar to that of nAg in $H_2O$. When calculating the hydrodynamic diameter of nAg, we measured the predominant peak only and excluded the minor peak around 8 nm which presumably represented proteins (Figure S3A). Furthermore, we performed this experiment with different concentrations of FBS (5, 10, 15, and 20%) in medium with nAg at 8 $\mu$g/mL, and then the hydrodynamic diameter was determined at 0 and 24 h. As shown in Figure S3B, the increase of FBS

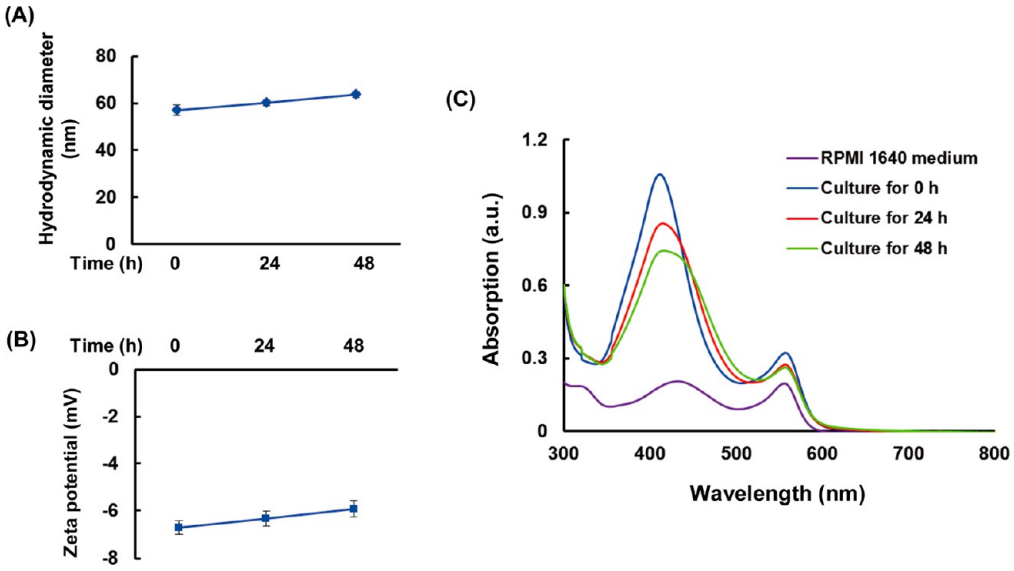


**Figure 4. Characterization of nAg in culture medium. Culture medium was collected at 0, 24, and 48 h from plates after MEL cells were exposed to 8 $\mu$g/mL nAg. After centrifugation to pellet cells, the supernatants were subject to the analyses of hydrodynamic diameter (A), zeta potential (B), and UV−visible spectrum (C) of nAg. A dominant absorption peak of nAg is at 400 nm, and the peak at 550 nm represents the absorption of phenol red.**

concentration did not significantly alter the hydrodynamic diameter of nAg at 0 and 24 h. These results together demonstrated that proteins from the FBS had little influence on the hydrodynamic diameter of nAg in medium. As the data of the hydrodynamic diameter, zeta potential, and UV−visible spectrum of nAg in medium for 0, 24, and 48 h revealed (Figure 4A−C), nAg particles were stable with a slight agglomeration in cell exposure conditions at concentrations used in our experiments.

To interpret the influence of nAg exposure on cell growth and viability of MEL cells, we employed two methods, that is, direct cell number counting and the Alamar Blue assay. As the results of cell number counting indicated in Figure 5A, the half maximal inhibitory concentration ($IC_{50}$) was around 12 $\mu$g/mL for MEL cells upon exposure to nAg for 24 h. nAg at 8 $\mu$g/mL had no effect on cell number, while the number was reduced by approximately 40% when nAg reached 10 $\mu$g/mL (Figure 5A, $P < 0.01$). Alamar Blue assay is an ideal approach to quantitatively measure proliferation and metabolic status of cells, especially for cells cultured in suspension (such as MEL cells used in the current study).[27,28] Similar to the results of cell number counting, the Alamar Blue assay suggested that the concentration of half maximal inhibition on cell viability was greater than 10 $\mu$g/mL (Figure 5B, $P < 0.01$). In contrast to nAg, MEL cells are fairly vulnerable to Ag ions (in $AgNO_3$) at even very low concentrations (0.08 $\mu$g/mL), with significant reduction in cell viability in comparison to the control (Figure 5C, $P < 0.05$), and cell viability was dramatically impaired by Ag ions at 1.2 $\mu$g/mL (Figure 5C, $P < 0.001$). Although Ag ions could impair cell viability at concentrations of 0.08 and 0.8 $\mu$g/mL, globin gene transcription was not significantly affected compared to nAg at 8 $\mu$g/mL (Figure 5D), suggesting that nAg-induced inhibition of RNA transcription could be separated from the cytotoxicity pathway triggered by Ag ions, and the localization and the intracellular concentration of Ag should play a major role in conducting these effects in MEL cells.

There has been much discussion on the sources of nAg-mediated biological effects from Ag ions, "particle-specific" effects, or both; no conclusive answer is reached to date. The addition of Ag ions could be quickly precipitated by ample Cl ions in the *in vitro* transcriptional system (as described in the Methods). We therefore could not perform experiments such as runoff and run-on assays with $AgNO_3$. However, we circumvented this issue by looking at the portions of Ag ions and nAg particles inside the cells using the technique of cloud point extraction.[29] We followed this optimized method of cloud point extraction for separation of nAg particles and Ag ions in mammalian cells (a schematic diagram described in Figure 6A), as previously described.[29] We demonstrated that over 82.1% of Ag existed in the form of nanoparticles, with less than 17.9% as Ag ions inside MEL cells (Figure 6B). Similar to our finding, Yu and colleagues documented that about 10.3% of Ag presented as ions in exposed Hep G2 cells. The slight difference in the ratio of Ag dissolution might be due to different physiochemical properties of nAg used in these two studies and different cell type. Nonetheless, our finding confirmed that nAg provided "Trojan horse" effects that could conduct either ion effects or particle effects, or both, and both nAg particles and Ag ions might potentially exert influences on cells, consistent with recent findings that nAg particles and Ag ions together contribute

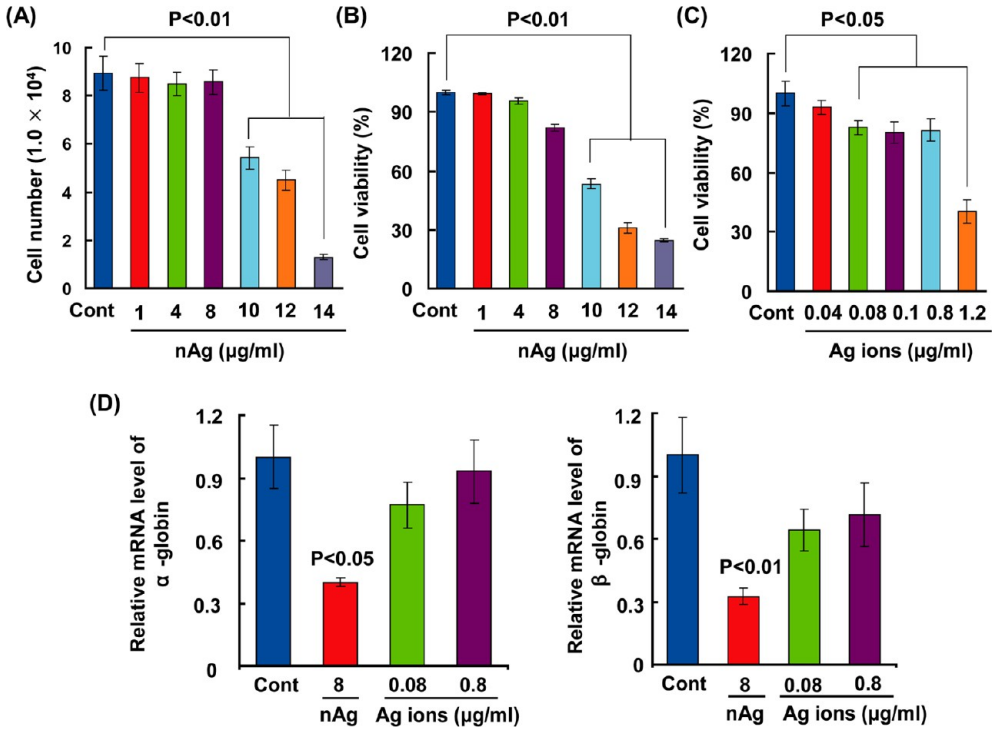


**Figure 5. Cell growth and viability assessments and globin expression upon Ag ions and nAg at various concentrations. (A) Cell growth was determined by cell counting in MEL cells upon exposure to nAg for 24 h ($n = 4$). (B) Cell viability was assessed with the Alamar Blue assay in MEL cells upon exposure to nAg for 24 h ($n = 6$). (C) Cell viability was evaluated with the Alamar Blue method in MEL cells treated with Ag ions for 24 h ($n = 6$). (D) Relative expression of $\alpha$-globin and $\beta$-globin mRNAs determined by qRT-PCR in cells upon Ag ions and nAg for 24 h ($n = 4$).**

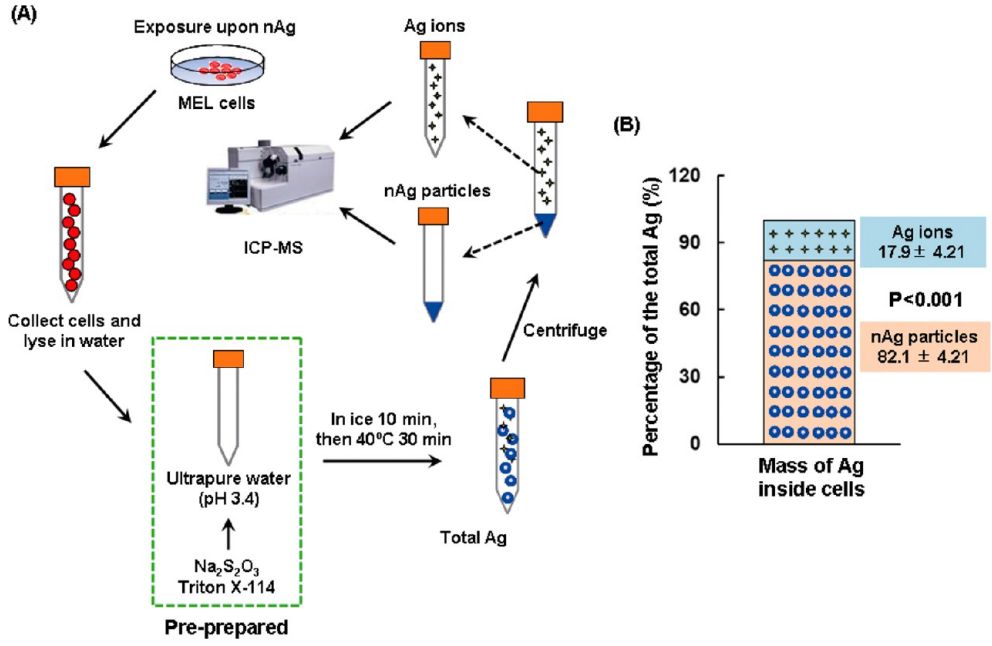


**Figure 6. Portions of nAg particles and Ag ions inside MEL cells. (A) A schematic diagram for the method of cloud point extraction of nAg particles. (B) Percentages of nAg particles and Ag ions of the total Ag mass inside MEL cells ($n = 6$).**

to the overall cytotoxicity.[16,30−32] "Trojan horse" means a vehicle or carrier to transport ions/particles or other toxic substances through membrane barrier, and then releases these substances inside cells or organisms.[33] In the field of nanoscience, nanomaterials such as ZnO and CuO nanoparticles could enter cells through endocytosis, and nanomaterials inside cells could undergo dissolution and release their corresponding ionic species.[34,35] In contrast, the ionic forms of these materials could not enter the cells freely due to the presence

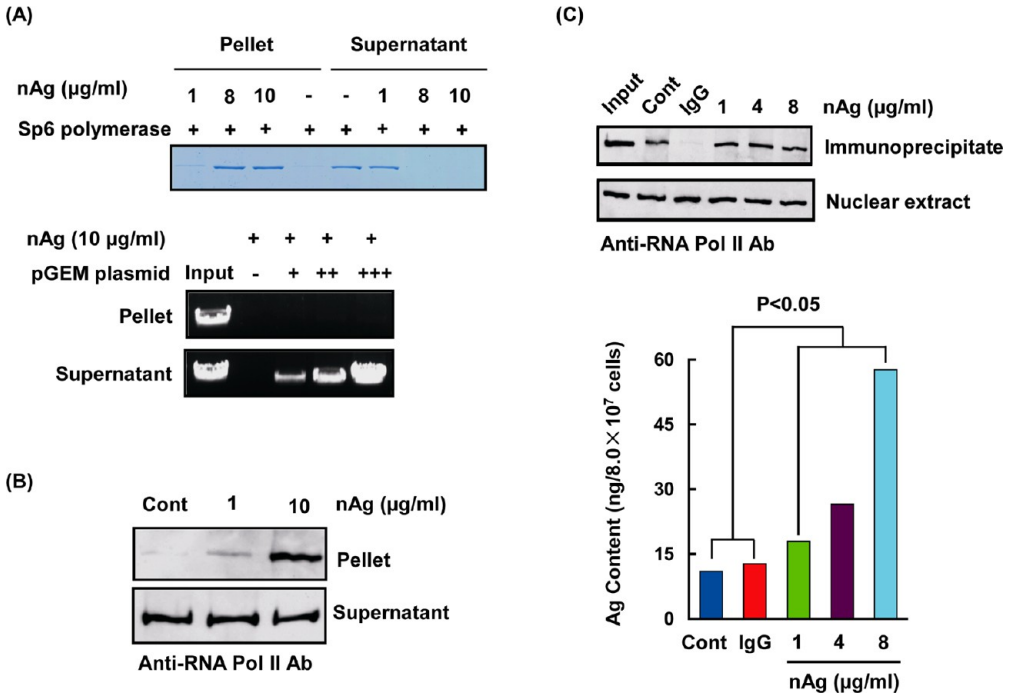


**Figure 7. A direct interaction between RNA polymerase and nAg. (A) Pull-down assay of nAg with Sp6 RNA polymerase or DNA template. The level of Sp6 RNA polymerase distributed in the two fractions of supernatants and pellets was assessed by SDS-PAGE followed by coomassie blue staining (the upper panel). The amount of DNA distributed in the two fractions was determined using agarose gel electrophoresis (the lower panel). The mass of linearized pGEM plasmid used in the assay is marked as 1 cross (+, 0.5 $\mu$g), 2 crosses (++, 1 $\mu$g), and 3 crosses (+++, 2 $\mu$g). (B) Binding of RNA polymerase to nAg in MEL nuclear extracts. Nuclear extracts from MEL cells were incubated with or without nAg. After centrifugation, the concentrations of RNA polymerase in supernatants and pellets were determined by Western blotting. (C) Immunoprecipation assessment of the binding between nAg and RNA polymerase in MEL cells. After dialysis, the nuclear extracts were immunoprecipitated with an anti-RNA polymerase II Ab. RNA polymerase II was evenly distributed in nuclear extracts, and the anti-RNA polymerase II Ab could potently precipitate RNA polymerase II into the immunoprecipitates (the upper panel). The mass of coimmunoprecipitated nAg on RNA polymerase II was quantified using the ICP-MS assay (the bar graph). Normal IgG was used as a negative control.**

of membrane barrier.[36] The "Trojan horse" model therefore delineates the potential mechanisms and possible sources responsible for the cytotoxicity of nanomaterials.[37−39]

In an attempt to further elucidate the molecular basis of the inhibitory effect of nAg on RNA polymerase-conducted transcription, we teased apart a potential interaction between nAg and RNA polymerase in an acellular system and in cells. We first carried out a pull-down assay of nAg with Sp6 polymerase, and the coomassie blue staining of SDS-PAGE gels showed that a large amount of Sp6 RNA polymerase was precipitated in the pellets, whereas fewer proteins were left in the corresponding supernatants from the reaction system with nAg at 1, 8, and 10 $\mu$g/mL, particularly at the latter two concentrations (Figure 7A). In contrast, no template DNA was precipitated in the pellets; all DNA templates remained in the supernatants (Figure 7A). These observations indicated that nAg could potentially bind to RNA polymerase but not to DNA in the *in vitro* transcriptional system, leading to impaired Sp6 RNA polymerase activity and reduced RNA synthesis as a result (Figure 3A,B). We thereafter addressed a possible interaction of nAg with RNA polymerase in erythroid cells by performing a pull-down assay with nuclear extracts from MEL cells in the presence of nAg. The Western blot analysis showed that RNA polymerase II was precipitated into the pellets by nAg at 1 and 10 $\mu$g/mL, especially at 10 $\mu$g/mL, with reduced RNA polymerase II concentrations in supernatants compared to the control (Figure 7B). Furthermore, to confirm the finding that nAg binds to RNA polymerase, we studied the *in situ* interaction between nAg and RNA polymerase using immunoprecipitation with an anti-RNA polymerase II antibody (Ab). The Western blot analysis indicated that RNA polymerase II was successfully precipitated by the Ab from the nuclear extracts in all groups with or without nAg treament; however, the ICP-MS assay showed that Ag was present only in the coimmunoprecipitated proteins from nAg-treated cells but not in control cells, and the Ag amount extracted from the coimmunoprecipitated proteins significantly increased from 1 to 4 and 8 $\mu$g/mL in a dose-dependent manner (Figure 7C, $P < 0.05$). The known pathways for cellular uptake of Ag ions rely on limited transport through the copper transport protein and sodium channels,[40,41] and no interruption of Ag ions has been demonstrated on other ion channels, such as magnesium, which is required for polymerase activity. Together, these

(A)

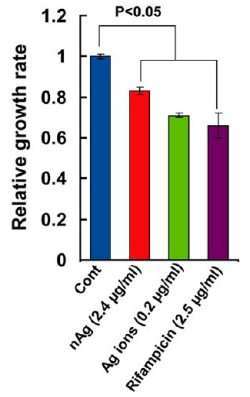


(B)

| Relative gene expression | | nAg (2.4 μg/ml) | Ag ions (0.2 μg/ml) | Rifampicin (2.5 μg/ml) |
|---|---|---|---|---|
| Category | Gene name | | | |
| Carbon and energy metabolism | *lacA* | ↓* | — | ↓↓* |
| | *ndh* | ↓* | — | ↓↓* |
| Outside membrane formation | *ompC* | ↓↓* | — | ↓↓* |
| | *ompF* | ↓* | — | ↓↓* |
| | *lamB* | ↓↓* | — | ↓* |
| Ribosome biosynthesis | *rpsE* | ↓↓* | — | ↓↓* |
| | *rpiO* | ↓↓* | — | ↓↓* |
| Stress-responsive reaction | *icd* | ↓* | — | ↓↓* |
| | *hybO* | ↓↓* | — | ↓↓* |
| | *hypB* | ↓↓* | — | ↓↓* |

**Figure 8. nAg repressed gene expression in E. coli cells. (A) Relative bacterial growth rate in response to 2.4 μg/mL nAg, 0.2 μg/mL Ag ions, or 2.5 μg/mL rifampicin. E. coli cells were collected at 9 h and determined for absorption at 600 nm ($n = 4$). (B) Assessment of mRNA levels for vital genes in E. coli cells treated with 2.4 μg/mL nAg, 0.2 μg/mL Ag ions, or rifampicin at 2.5 μg/mL for 9 h ($n = 4$). 16S rRNA was used as a loading control. These genes code proteins involved in carbon and energy metabolism (*lacA* and *ndh*), outside membrane formation (*ompC*, *ompF*, and *lamB*), ribosome biosynthesis (*rpsE* and *rpiO*), and stress-responsive reaction (*icd*, *hybO*, and *hypB*). One arrow (↓) represents ~0.5-fold decrease, and 2 arrows (↓↓) represent ~1-fold decrease. Dash (—) represents no statistically significant change. Asterisk (*) represents $P < 0.05$.**

results demonstrated that nAg could directly bind to RNA polymerase, which resulted in a robust inhibition of RNA polymerase activity.

In fact, inhibition of microbial or viral RNA polymerase activity has long been used as a strategy against invading pathogens.[42,43] For example, the antibacterial agent rifamycin predisposes bacterial cells to death by binding to the active center of bacterial RNAP and repressing RNA elongation.[44] We also looked into the effect of nAg on mRNA transcription in *E. coli* cells, and to better elucidate the potential inhibitory effect, we avoided dramatic cell death and chose nAg concentration of 2.4 μg/mL, at which nAg caused no great toxicity to cell growth after treatment for 9 h (i.e., at sublethal concentrations; Figure 8A). As shown in Figure 8B and Table S2, nAg suppressed the transcription of many vital genes in *E. coli* cells, such as *lacA*, *ndh*, *icd*, *ompC*, *ompF*, *lamB*, *hypB*, *hybO*, *rpsE*, and *rpiO*, as the mRNA levels of these genes were decreased by 0.5−1.0-fold in cells treated with nAg at 2.4 μg/mL for 9 h ($P < 0.05$). Rifampicin is a clinically applied antibiotic belonging to the rifamycin group, which was used here as a positive control and exerted substantial inhibition on cell growth and gene expression (Figure 8 and Table S2, $P < 0.05$). Although Ag ions at 0.2 μg/mL could diminish cell growth greater than nAg at 2.4 μg/mL (Figure 8A), no significant repression on transcription for these genes was found (Figure 8B and Table S2). These data suggested that Ag ions induced a different pathway, a cytotoxicity pathway, instead of transcription inhibition, and nAg-dependent suppression of RNA transcription could be separated from Ag ion-mediated toxicity to *E. coli* cells. To this end, the antimicrobial properties of nAg might also be attributed to its binding to RNA polymerase and consequential suppression of RNA polymerase-dependent RNA transcription; however, this finding has not yet been reported previously.

A recent study from our research group demonstrated that nAg exhibited a robust ability to cross the placental barrier, and a substantial amount of Ag accumulated in the embryonic hematopoietic organ fetal liver at E14.5 from mice treated with nAg.[45] Erythroid progenitor cells are the predominant cells in fetal liver around E14.5, and it is an optimal model for the study of embryonic definitive erythropoiesis.[22,46] To closely evaluate the inhibition of nAg on RNA transcription in erythroid cells *in vivo*, we assessed the biological performances of nAg in fetal liver cells. We administrated male and female mice with nAg or $AgNO_3$ *via* intraperitoneal injection, and after exposure for 4 weeks, mice were mated as previously described.[45] Embryos were separated, and fetal livers and embryonic blood were collected on E14.5. We observed pronounced embryonic developmental retardation in embryos from 22 μg/kg nAg-treated mice, with nearly 40% reduction of embryonic weight compared to those from the other groups (Figure 9A, $P < 0.001$). The number of embryos per litter was not significantly changed among these groups (data not shown). Similar to our results, recent studies also demonstrated that nAg could significantly impede larvae development of *Chironomus riparius* and embryonic development of zebrafish.[47,48] When dissecting the embryos, we observed pale fetuses from mice treated with 22 μg/kg nAg, indicative of anemia in these fetuses, compared to those from the control mice (Figure 9B). No significant phenotypes were observed in embryos from 108 μg/kg nAg-treated mice, supporting our previous finding that nAg administration in mice at 22 μg/kg had a greater ability to cross the placental barrier, while nAg at a higher

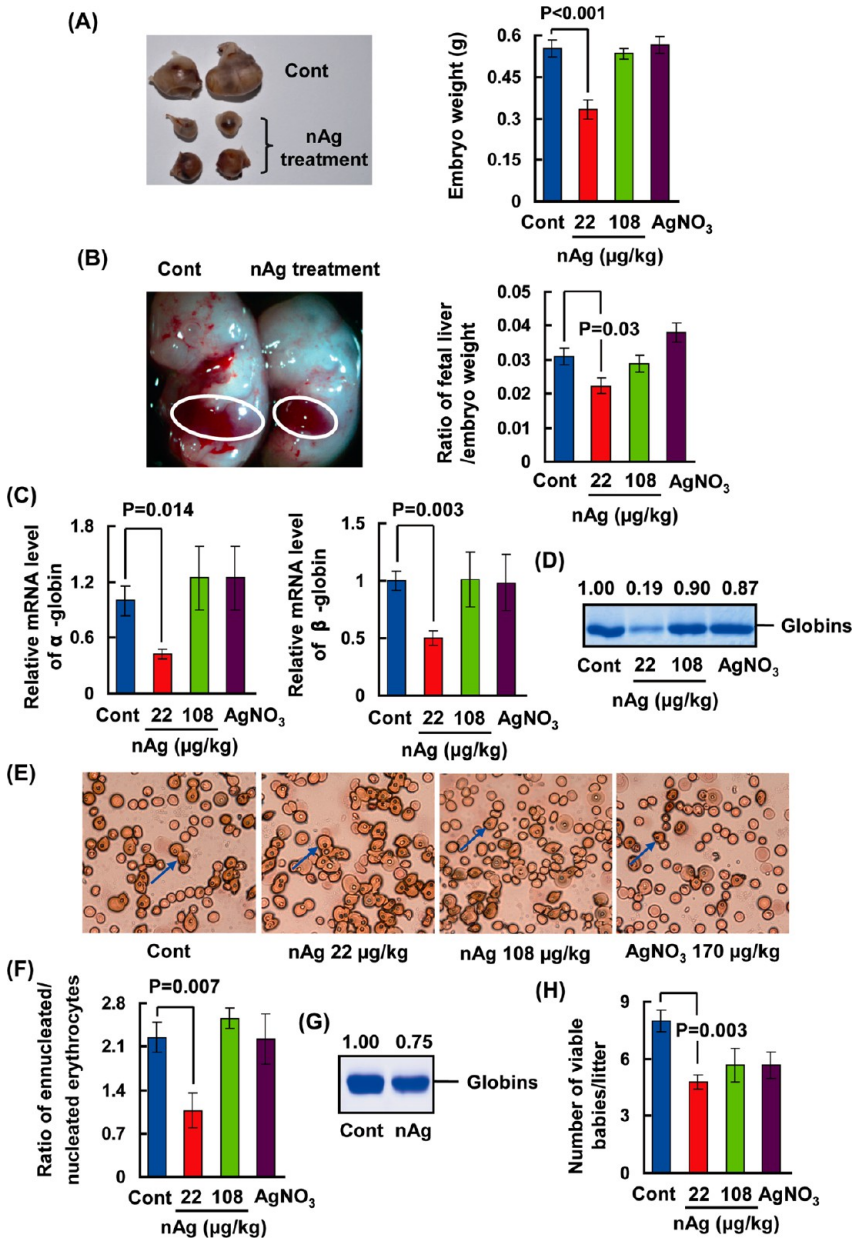


**Figure 9. nAg repressed hemoglobin transcription in fetal livers at E14.5 in mice. (A) Representative images of embryos from mice with or without nAg treatment (22 $\mu$g/kg body weight). Embryo weights are shown in the bar graph ($n$ = 36−40). (B) Representative images of fetuses from mice treated with 22 $\mu$g/kg body weight nAg in comparison to the control. The white ovals indicate fetal livers. The bar graph shows the ratio of fetal liver weight/embryo weight ($n$ = 18−34). (C) Expression of globin mRNAs in fetal livers. The mRNA levels were assessed by qRT-PCR and were normalized to eIF2$\alpha$. (D) Concentrations of globin proteins in fetal liver. Protein levels were assayed by SDS-PAGE with coomassie blue staining. (E) Blood smears of embryonic peripheral blood stained with alizarin red S and Giemsa solutions. Blue arrows indicate nucleated primitive yolk sac-derived erythrocytes. The original magnification, ×400. (F) Ratio of ennucleated and nucleated erythrocytes in embryonic peripheral blood ($n$ = 6−9). (G) Hemoglobin content in embryonic peripheral blood from mice with or without nAg treatment (22 $\mu$g/kg body weight). Protein concentrations were determined by SDS-PAGE with coomassie blue staining. (H) Numbers of viable fetuses per litter after birth. Male and female mice were mated after exposure to nAg, and fetuses were given birth. The baby mice were counted if they survived ($n$ = 6−9). The intensity of protein bands was quantified with the software Image J, and the hemoglobin concentration in the PBS group is defined as 1. The normalized values are shown above the images.**

concentration could diminish their own ability to translocate from maternal blood into embryonic blood *via* the placental barrier, presumably due to agglomeration under the biological setting.[45] In agreement with this finding, high concentrations of nAg could significantly agglomerate and aggregate in the MEL cell exposure system, as the hydrodynamic diameter greatly expanded after nAg concentration reached 22 $\mu$g/mL (Figure S4, $P < 0.001$). We further examined the weight of fetal livers and found that the relative weight of fetal liver normalized to fetal body weight was largely diminished in 22 $\mu$g/kg nAg-treated mice compared to the other groups (Figure 9B, $P < 0.05$). These observations suggested that *in vivo* nAg exposure led

(A)

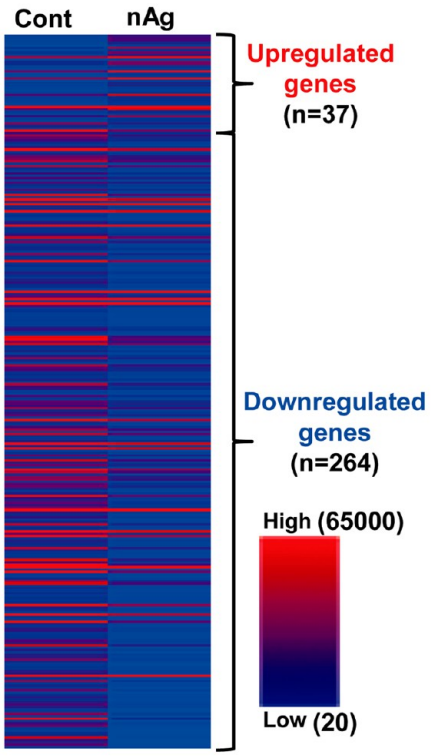


(B)

| Gene symbol | Gene Description | Fold change |
|---|---|---|
| **Erythroid genes** | | |
| Acadm | Acyl-Coenzyme A dehydrogenase, medium chain | -2.02 |
| Acox1 | Acyl-Coenzyme A oxidase 1, palmitoyl | -2.60 |
| Apoc2 | Apolipoprotein C-II | -2.15 |
| Aqp1 | Aquaporin 1 | -2.27 |
| Aqp8 | Aquaporin 8 | -10.91 |
| Aqp11 | Aquaporin 11 | -2.75 |
| Atf5 | Activating transcription factor 5 | -2.51 |
| Cdh1 | Cadherin 1 | -2.25 |
| C1r | Complement component 1, r subcomponent | -2.95 |
| Col15a1 | Procollagen, type XV | -2.72 |
| Col6a1 | Procollagen, type VI, alpha 1 | -2.32 |
| Cyp2a12 | Cytochrome P450, family 2, subfamily a, polypeptide 12 | -7.94 |
| Dffa | DNA fragmentation factor, alpha subunit | -6.28 |
| Esrra | Estrogen related receptor, alpha | -2.09 |
| Gamt | Guanidinoacetate methyltransferase | -2.46 |
| Gcgr | Glucagon receptor | -2.56 |
| Gpld1 | Glycosylphosphatidylinositol specific phospholipase D1 | -3.81 |
| Hp | Haptoglobin | -2.74 |
| Lcn2 | Lipocalin 2 | -2.06 |
| Lgals9 | Lectin, galactose binding, soluble 9 | -2.49 |
| Rab3d | RAB3D, member RAS oncogene family | -2.49 |
| Sct | Secretin | -2.44 |
| **Ion transport** | | |
| Fxyd1 | FXYD domain-containing ion transport regulator 1 | -2.35 |
| Fxyd3 | FXYD domain-containing ion transport regulator 3 | -5.49 |
| Slc36a2 | Solute carrier family 36, proton/amino acid symporter | -3.61 |
| Slc38a3 | Solute carrier family 38, member 3 | -6.29 |
| Slc39a5 | Solute carrier family 39, metal ion transporter | -3.00 |
| Slc44a3 | Solute carrier family 44, member 3 | -2.22 |
| Tmprss6 | Transmembrane serine protease 6 | -2.81 |
| **Iron and heme genes** | | |
| Hpxn | Hemopexin | -3.32 |
| Ltf | Lactotransferrin | -2.16 |
| **Antioxidant genes** | | |
| Hspb8 | Heat shock protein 8 | -4.84 |
| Selenbp1 | Selenium binding protein 1 | -2.33 |

**Figure 10. Microarray analysis of gene expression changes in fetal liver cells in embryos from 22 $\mu$g/kg nAg-treated mice compared to those in embryos from the control mice. (A) Heat map representing the differentially expressed genes upon nAg exposure. (B) Representative differentially expressed genes with functional descriptions.**

to a significant impairment of embryonic development coupled with fetal anemia. We thereafter surveyed hemoglobin concentrations in fetal liver cells, and the qRT-PCR analysis showed a significant decline of both $\alpha$-globin and $\beta$-globin mRNAs in fetal liver cells from 22 $\mu$g/kg nAg-treated mice, compared to those from the control mice (Figure 9C, $P < 0.05$). Consistent with the qRT-PCR results, the globin protein concentration was greatly reduced in fetal liver cells from the mice treated with 22 $\mu$g/kg nAg compared to that from the other groups (Figure 9D). The staining of embryonic peripheral blood smears indicated that the majority of E14.5 peripheral red blood cells were enucleated erythrocytes in the embryos from control mice and 108 $\mu$g/kg nAg-treated or $AgNO_3$-treated mice; in stark contrast, a great proportion of peripheral red blood cells were larger nucleated primitive yolk sac-derived erythrocytes in embryos from 22 $\mu$g/kg nAg-treated mice (Figure 9E). The ratio of enucleated erythrocytes to nucleated erythrocytes decreased significantly in embryos from mice with 22 $\mu$g/kg nAg treatment, compared to that in the other groups (Figure 9F, $P < 0.05$), suggesting that the definitive erythropoiesis was attenuated and the primitive erythropoiesis was prolonged to compensate. Moreover, the hemoglobin content in embryonic peripheral blood evidenced by coomassie blue staining was reduced by about 25% in embryos from 22 $\mu$g/kg nAg-treated mice compared to that in embryos from control mice (Figure 9G). Additionally, the microarray analysis revealed that a number of genes were repressed in fetal liver cells in embryos from 22 $\mu$g/kg nAg-treated mice compared to that in embryos from the control mice. There were a total of 301 differentially expressed genes with 37 upregulated genes and 264 downregulated genes and, of these downregulated genes, many are involved in the regulation of erythropoiesis, such as *Aqp1*, *Cdh1*, and *Hpxn*[22,49] (Figure 10), suggesting a significant inhibition on transcription of a variety of vital genes in fetal liver cells upon exposure to nAg. This observation was similar to the finding from a previous study that demonstrated the downregulation of many genes in fish cells treated with nAg through the microarray analysis.[50] These results collectively suggested a large reduction of erythropoiesis in fetal livers in embryos upon exposure to nAg, and the prominent repression of gene transcription in erythroid cells was likely the molecular basis for nAg-induced fetal anemia and developmental retardation.

Previous studies have indicated that nanomaterials, such as carbon nanotubes, $TiO_2$, and $SiO_2$ nanoparticles and quantum dots, are able to transport through the placental barrier and accumulate in the fetus,[51−53] and developmental toxicity of nanomaterials might

stem from the nanoparticle-stimulated oxidative stress to placenta and fetus and the released metal ion-mediated detrimental effects as well.[17,51−55] Our recent study demonstrated that no significant histological alterations were observed in the placentas from mice treated with 22 $\mu$g/kg nAg,[45] suggesting that the embryonic impairment did not result from damage in the placenta. We here demonstrated that nAg reduced hemoglobin content in erythroid progenitor cells by directly inhibiting globin gene transcription coupled to embryonic anemia (Figure 9), which, at least partially, accounted for developmental retardation of the embryos. Meanwhile, nAg-mediated overall inhibition on RNA transcription would lead to general cell proliferation deficit, which should also contribute to the diminishment of embryo development. To follow the fate of fetuses with developmental impairments upon nAg exposure, we carried out *in vivo* nAg exposure in another group of mice that were allowed to give birth to babies. The average number of viable babies per litter was significantly reduced in mice upon 22 $\mu$g/kg nAg exposure compared to control mice (8.0 *vs* 4.8; Figure 9H, $P < 0.05$), confirming the finding of embryonic developmental impairments as described above. No abnormal developmental parameters (such as activity, diet, and complete blood count indexes) were observed in those surviving mice from the parental mice with 22 $\mu$g/kg nAg administration, and no Ag was detected in a wide spectrum of organs when mice were 8 weeks old (data not shown), likely due to a growth-induced dilution of nanomaterials.[56]

Embryonic development, hemoglobin content in fetal liver cells and the constituents of peripheral red blood cells were not significantly changed in embryos from 108 $\mu$g/kg nAg-treated mice or $AgNO_3$-treated mice compared to control mice (Figure 9). In terms of Ag ions, because they can bind to thiol groups in proteins and chloride (which are plenty inside body fluid and blood) to form a silver-thiol complex and undissolvable AgCl, most Ag ions will quickly lose its ionic effects. In contrast, Ag in nanoparticle form can constantly dissolve and travel to the other places. Additionally, it is rather difficult for Ag ions to cross cellular membrane and the biological barriers,[40,41] and our recent study also demonstrated that the bioavailability of Ag ions is minimal to mammalian cells in mice.[45] Nonetheless, a mild embryonic toxicity was observed in mice challenged by nAg or Ag ions both at 108 $\mu$g/kg, as the numbers of viable babies in these two groups were reduced compared to the control, despite the absence of statistical significance (Figure 9H, $P > 0.05$). This suggests some Ag could still gain access to the embryos through the placenta.

Additionally, previous studies have demonstrated that nAg could enter cells and induce intracellular reactive oxygen species (ROS) generation.[16,57,58] ROS might then cause secondary injuries, such as a blockade of signal transduction cascades, protein degradation, and cytoskeleton disruption.[59,60] In the current study, we did not observe significant ROS induction in MEL cells upon nAg treatment at various concentrations over time (Figure S5A); however, there was still significant inhibition on globin transcription (Figure S5B, $P < 0.05$), suggesting the inhibition of nAg on RNA polymerase activity is independent of ROS.

To date, the mechanisms responsible for nAg-induced antimicrobial properties and nAg-mediated toxicity to organisms keep elusive. Overall, studies support that both the "nanoparticle-specific" effects and toxicity of Ag ions are involved in incurring damage to cells;[18,61] however, regarding the relative contribution of "nanoparticle-specific" effects and toxicity of Ag ions to the overall toxicity, it is rather difficult to conclude. Release of Ag ions under biological settings could account for the majority if not all of the toxicity of nAg to cells,[17,62,63] whereas whether nAg *per se* exerts direct "particle-specific" effects remains inconclusive, and there is always intense debate on whether the toxicity of nAg is due to Ag ion-mediated effects or particle-stimulated effects. Since the release of Ag ions from nAg behaves in a dynamic fashion, which can happen outside cells and inside cells and also closely relies on the environment,[63−65] it is hard to differentiate these two sources of effects. Some studies indicated that nAg was more toxic than equivalent concentrations of Ag ions due to the release of Ag ions, and nAg particles and Ag ions together contributed to cytotoxicity.[66,67] Meanwhile, other studies also demonstrated that nAg particles revealed greater toxicity due to shape- and surface-reactivity, despite lower rates of dissolution.[20] In contrast, there are also studies demonstrating that the toxicity of nAg is solely due to released Ag ions. For example, a recent study demonstrated that the antimicrobial activity primarily derived from released Ag ions, and ruled out the direct contribution of "particle-specific" effects in *E. coli* cells.[68] Nonetheless, the size, shape and other properties such as agglomeration and surface coating have been demonstrated to play an important role in executing nAg's antimicrobial actions and cellular toxicity.[3,20,57,69,70] Thus, the relative contribution of released Ag ions and "particle-specific" effects largely relies on the physicochemical properties of nanomaterials, the exposure environment, and types of organisms used in studies,[25,64,71] and it is rather complex to dissect the relative contribution of "nanoparticle-specific" effects and toxicity of Ag ions. In the current study, we demonstrated that nAg exhibited a robust inhibition on RNA polymerase activity and RNA transcription through direct Ag binding to RNA polymerase, which could be an alternative pathway in addition to the effects of Ag ions. Without particle formulation, Ag ions could not get inside of cells freely, and therefore, in this regard, the "Trojan horse" effects make the responses much stronger

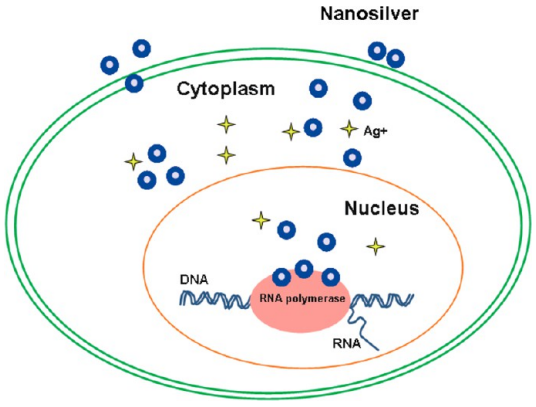


**Figure 11. Schematic diagram depicting nAg-induced RNA polymerase-silver binding and RNA transcription inhibition in erythroid progenitor cells.**

because of the great bioavailability of nAg and the toxicity of dissolved ions. Our data in the current study suggested that the particle effects could be the predominant mediator in conducting biological influences under relatively low concentrations of nAg exposure to erythroid cells.

## CONCLUSIONS

This report overall confirms the indisputable effects of nAg-induced inhibition on transcription through direct Ag binding to RNA polymerase in erythroid cells, which is novel and different from the cytotoxic effects of Ag ions. As to the relative contribution of particle or ion effects, it is still debatable; however, nAg provides "Trojan horse" effects that could execute either ion effects or particle effects, or both, on cells after cellular uptake, as illustrated in Figure 11. The combined data from the current study would subserve the understanding of nAg's cellular toxicity and antimicrobial properties, and also provide additional insights into the mechanisms underlying the developmental toxicity of nanomaterials.

## MATERIALS AND METHODS

**Characterization of nAg.** Polyvinylpyrrolidone (PVP)-coated nAg particles were either purchased from Shanghai Huzheng Nanotechnology Co., Ltd., China, or nanoComposix, Inc., U.S.A. nAg solution was purified by centrifugation and redispersion in deionized $H_2O$ to remove Ag ions followed by storage in the dark at 4 °C. Purified particles were characterized by transmission electron microscopy (TEM, Hitachi H-7500, Japan). Hydrodynamic diameter and zeta potential were determined using a Zetasizer (Malvern Nano series, Malvern, U.K.), and the absorption spectrum was measured by a UV−vis spectrometry (Beckman coulter, U.S.A.).

**Cell Culture, nAg Treatments, and Inductively Coupled Plasma Mass Spectrometry (ICP-MS) Analysis.** MEL cells were purchased from the Cell Resource Center of the Institute of Basic Medical Sciences (CAMS), China. Cells were cultured in suspension in RPMI 1640 medium (Gibco) supplemented with 10% fetal bovine serum (FBS; Hyclone), 2 mM L-glutamine and 100 U/mL penicillin/streptomycin (Hyclone). To initiate differentiation, MEL cells were induced with 1.5% dimethyl sulfoxide (DMSO; Solarbio, China). Cell growth and viability were determined by direct cell number counting and the Alamar Blue assay, respectively. Briefly, after induction for 3 d, MEL cells were seeded into 24-well plates with $8.0 \times 10^4$ cells/well or 96-well plates with $3.0 \times 10^4$ cells/well. Cells were then treated with nAg or Ag ions at various concentrations for 24 h, followed by cell number counting for 24-well plates or the Alamar Blue assay for 96-well plates, respectively. Cell numbers were counted with a cytometer. Regarding the Alamar Blue assay, after 24 h treatment, resazurin (Sigma) was added into culture media at a final concentration of 10% (V/V). Cells were cultured for another 2 h at 37 °C, and thereafter, fluorescence intensity was assessed at an excitation wavelength of 530 nm with an emission wavelength of 590 nm.

With respect to detection of intracellular Ag content and assessment of globin gene transcription, MEL cells were cultured with DMSO for 3 d and then exposed to nAg for an additional 3 d. Regarding nuclear run-on assay and immunoprecipitation experiment, nAg was added at the beginning when MEL cells were induced to differentiate with DMSO, and culture continued for 4 d prior to collection for experiments. Ag mass inside cells was assessed using the ICP-MS (Agilent 7500) method according to the protocol as previously described.[72]

**Radioactive Labeling of RNAs and qRT-PCR Analysis.** After induction with DMSO for 3 d, MEL cells were exposed to nAg at various concentrations for 48 h and then labeled with $^{32}P$ according to the protocol as described previously.[73] Briefly, culture medium was first replaced with phosphate-free Dulbecco's modified Eagle's medium (Hyclone) supplemented with 10% FBS, and cells were cultured for 1 h. [$^{32}P$]orthophosphate was then added at a final concentration of 20 $\mu$Ci/mL, and cells were incubated for an additional 2 h. Culture medium was replaced with nonradioactive RPMI 1640 medium supplemented with 10% FBS, and cells were further incubated for 2 h before collection. Total RNAs were purified from these cells with TRIzol reagent (Invitrogen). Thereafter, 20 $\mu$g of total RNAs from each sample were run in a 1% agarose formaldehyde gel, and radioactive bands were detected by autoradiography. qRT-PCR was performed to assess relative expression of globin genes as described previously.[74] Here, eIF2$\alpha$ was used as an internal control. Primers for PCR are provided in Table S3.

**Run-Off Transcription Assay and Nuclear Run-On Assay.** Run off transcription assay was carried out using an *in vitro* transcription system according to the manufacturer's instructions (Promega). RNA synthesis was initiated with the addition of 4 $\mu$Ci [$\alpha$-$^{32}P$]UTP into the transcription buffer (40 mM Tris-HCl, pH 7.9, 6 mM $MgCl_2$, 2 mM spermidine, 10 mM NaCl) with or without nAg at various concentrations. Reaction lasted for 3 h at 37 °C, and DNA template was digested using 1 U RNase-free DNase (Promega). Radio-labeled nascent transcripts were quantified by slot blot hybridization.

Nuclei were prepared from $1.0 \times 10^7$ MEL cells for each sample using a PROteoJET cytoplasmic and nuclear protein extraction kit (Fermentas). Nuclear run-on assay was performed essentially as described previously with some modifications.[75] Briefly, crude nucleus suspension was gently added into run-on buffer (40 mM Tris-HCl, pH 7.9, 6 mM $MgCl_2$, 2 mM spermidine, 10 mM NaCl, 0.4 mM each of ATP, GTP, and CTP, 10 mM DTT) with 200 $\mu$Ci [$\alpha$-$^{32}P$]UTP (10 $\mu$Ci/$\mu$L) and 15 $\mu$L ribonuclease inhibitor (40 U/$\mu$L, Promega). Reaction mix was incubated for 2 h at 30 °C. Thereafter, 60 $\mu$L RNase-free DNase (1 U/$\mu$L, Promega) was added to digest genomic DNA for 20 min at 37 °C. Run-on reaction was terminated by mixing with an equal volume of TRIzol reagent (Invitrogen). RNA purification was then performed with TRIzol reagent followed by isopropanol precipitation according to the manufacturer's instructions. RNAs were resuspended in RNase-free $H_2O$ and quantified by slot blotting and autoradiography.

**Slot Blot Hybridization.** Nitrocellulose membranes (Pall) were floated on RNase-free $H_2O$ for 5 min and soaked in 20× SSC for

20 min. Membranes were then inserted into a convertible filtration minifold system (Beijing Popular Science Instrument, China). Each well was washed once with 200 $\mu$L 20× SSC immediately before sample loading. Linearized plasmid DNA or PCR products were directly loaded onto membranes. Thereafter, membranes were dried at room temperature (RT) for 30 min and baked at 80 °C for 2 h.

Nascent RNAs with [$\alpha$-$^{32}$P] UTP labeling transcribed from runoff or run-on assay were used as hybridization probes. Prior to hybridization, membranes containing multiple DNA templates were cut into small sections with only one type of DNA template on each section. These membranes were prehybridized in 10 mL of hybridization buffer (50% formamide, 5× Denhardt's solution, 0.5% SDS, 5× SSPE and 100 $\mu$g/mL denatured herring sperm DNA) for 3 h at 42 °C, and thereafter hybridized with each RNA probe overnight in 10 mL of hybridization buffer at 42 °C. The membranes were washed twice with 2× SSC/0.1% SDS at RT for 5 min, and twice with 0.1× SSC/0.1% SDS at 68 °C for 15 min. Autoradiograph was visualized by exposing membranes to X-ray films at −20 °C with an intensifying screen.

**Interaction between nAg and Sp6 RNA Polymerase or DNA.** nAg at various concentrations and Sp6 RNA polymerase (4 $\mu$L, 20 U/$\mu$L, Promega) were mixed into transcription buffer (as described above) and incubated at 37 °C for 2 h. Mixtures were then centrifuged for 40 min at 20000 *g*. Pellets were washed twice with PBS, and bound proteins were dissolved in 20 $\mu$L PBS, subject to SDS-PAGE analysis. Interaction between nAg and DNA fragment was similarly assessed with various concentrations of DNA template.

**Interaction between nAg and RNA Polymerase II from MEL Cells.** MEL cells were cultured for 3 d in the presence of 1.5% DMSO. Nuclear extracts were prepared from 5.0 × $10^8$ cells as previously described.[76] Briefly, crude nuclei were resuspended and mixed in Buffer 1 (20 mM HEPES, pH 7.9 at 4 °C, 25% [v/v] glycerol, 1.5 mM $MgCl_2$, 20 mM KCl, 0.2 mM EDTA, 0.2 mM PMSF). Homogenates were gently vortexed, followed by the addition of Buffer 2 (the same as Buffer 1 except 1.2 M KCl), and were shaken for 30 min at 4 °C. Homogenates were finally centrifuged for 30 min at 25000 *g*. The resulting clear supernatants were dialyzed against Buffer 3 (20 mM HEPES, pH 7.9 at 4 °C, 20% [v/v] glycerol, 100 mM KCl, 0.2 mM EDTA, 0.2 mM PMSF) overnight. Dialysates were centrifuged at 25000 *g* for 40 min and supernatants were carefully removed and placed into new tubes. Nuclear extracts were added into the binding buffer (20 mM HEPES, pH 7.9 at 25 °C, 20% [v/v] glycerol, 100 mM KCl, 0.2 mM EDTA) in a final volume of 500 $\mu$L. Thereafter, nAg was added and tumbled at 30 °C for 2 h. The total reactions were centrifuged for 40 min at 20000 *g*. Pellets were washed twice with 1 mL of PBS, and bound proteins were dissolved in 20 $\mu$L of 1× SDS sample buffer followed by Western blotting. An anti-RNA Polymerase II Ab (1:200, Santa Cruz Biotechnology) was used.

**Immunoprecipitation.** MEL cells treated with or without nAg were cultured for 4 d in the presence of DMSO. Nuclear extracts from these cells were prepared according to the protocol described above and then incubated with 2 $\mu$g RNA polymerase II Ab or normal IgG. Thereafter, immunoprecipitates were collected with Gamma-Bind A Sepharose beads (GE Healthcare). Immunoprecipitated proteins were assessed by Western blot analysis, and coimmunoprecipitated nAg was quantified using ICP-MS. To avoid precipitation of nAg, speed of centrifugation for immunoprecipitation was lower than 3000 *g*.

**Bacterial Culture and Gene Expression Evaluation.** DH5$\alpha$ *E. coli* cells were purchased from Beijing Bomai De Technology Co., Ltd., China. A single colony from a Luria−Bertani (LB) agar plate was inoculated in LB broth and cultured for 1 h at 37 °C with shaking at 180 rpm. Culture was suspended in fresh LB broth and then treated with nAg at final concentrations of 1.2 and 2.4 $\mu$g/mL or rifampicin at 2.5 $\mu$g/mL. Thereafter, bacterial culture was monitored by assessing absorption at 600 nm (OD 600 nm). Total RNAs from *E. coli* cells were extracted using TRIzol reagent, and qRT-PCR was performed to assess gene expression. PCR primers are provided in Table S3.

**Animal Experiments and Blood Smear Staining.** All animal care and experimental protocols were approved by the Committee of Animal Care at the RCEES, Chinese Academy of Sciences. Male and female BALB/c mice (6 weeks old) were purchased from the Vital River Laboratories (China) and housed under sterile conditions. Animals were allowed to acclimatize for 7 d before experimentation. Mice were injected intraperitoneally with nAg at 22 $\mu$g/kg (in 200 $\mu$L) or 108 $\mu$g/kg (in 200 $\mu$L), or Ag ions at 108 $\mu$g/kg in $AgNO_3$ (in 200 $\mu$L) three times a week for 30 d. The blank control mice received PBS only. Male and female mice were mated immediately after the final injection. For timed pregnancies, animals were mated overnight, and female mice were examined for vaginal plugs the next morning. Noon of the day of vaginal plug appearance was considered to be day 0.5 postcoitum (E0.5). Pregnant mice were anaesthetized and embryos were dissected from uteri and weighed on day 14.5 of pregnancy (E14.5). Thereafter, E14.5 fetal livers were carefully removed from each embryo. Levels of globin mRNAs in fetal livers were analyzed by qRT-PCR. Hemoglobin concentrations in fetal livers were assessed by coomassie blue staining of SDS-PAGE gels. Meanwhile, embryonic peripheral blood was collected from embryonic carotid for blood smear and SDS-PAGE analyses. With respect to the work of the survival rate of embryos, fetuses were given birth.

Blood smears were prepared on slides with 2 $\mu$L embryonic peripheral blood and dried at RT for 2 h. Smears were fixed with methanol for 5 min, washed in $H_2O$, and stained with preheated hemoglobin working stain (10% phosphomolybdic acid: 7.7% alizarin red S, 1:3) for 10 min, followed by washing with $H_2O$. Slides were counterstained with Giemsa working stain and finally washed with $H_2O$. Slides were dried at RT and examined under a microscope. Numbers of enucleated and nucleated erythrocytes from each visual field were counted.

**Microarray Analysis.** Total RNAs were extracted from E14.5 fetal livers in embryos from 22 $\mu$g/kg nAg-treated mice and the control mice. The 32k mouse Genome Array microchips, containing 32256 probes representing about 25000 genes, were used. Microarray experiments and data analysis were performed at the CapitalBio, China, and the experimental procedure was similar to that as previously described.[77] Significance analysis of microarrays (SAM, version 3.02) was employed to determine the differentially expressed genes, which were defined by fold changes at either 2-fold greater or fewer than 0.5-fold in the nAg-exposed cells compared to the control with FDR < 0.01. These microarray data are available at NCBI GEO (accession no. GSE43331).

**Cloud Point Extraction of nAg Particles.** We recently established a customized protocol of cloud point extraction for separation of nAg particles and Ag ions in mammalian cells, and this method was successfully used to quantify nAg particles and Ag ions in Hep G2 cells.[29] We thus followed this method to quantify nAg particles and Ag ions in MEL cells with modifications.[29] To avoid possible dissolution of nAg by $HNO_3$ during pH adjustment, we prepared tubes with 9 mL of ultrapure $H_2O$ at pH 3.4 supplemented with 0.2 mL of $Na_2S_2O_3$ and 0.3 mL of Triton X-114 (TX-114) prior to collection of cells. After exposure to nAg at 8 $\mu$g/mL for 24 h, MEL cells were collected after a 3× wash with PBS, and lysed in 1 mL of ultrapure $H_2O$, followed by incubation in ice for 15 min. Thereafter, cell lysates were quickly added into the prepared tubes with 9 mL of $H_2O$ and incubated for 10 min in ice, followed by incubation in a water bath for 30 min at 40 °C. These tubes then were centrifuged at 3000 g for 5 min to facilitate phase separation. Finally, nAg particles were concentrated into TX-114-rich phase, and Ag ions were left in the aqueous phase. The mass of nAg particles and Ag ions was determined by ICP-MS.

To evaluate the possible dissolution of nAg by $HNO_3$ during the experiment of cloud point extraction, we determined the concentrations of Ag ions in the stock solution before and after cloud point extraction. Briefly, nAg from the stock solution was diluted in $H_2O$ to a concentration of 1 $\mu$g/mL, and then three aliquots of the diluted stock solution were immediately tested for Ag ion concentrations, and another three aliquots were subject to cloud point extraction. Concentrations of released Ag ions in the diluted nAg stock solution were measured using a silver/sulfide ion selective electrode (Van-Landon pHoenix, Houston, TX) as previously described.[78] Various concentrations

of Ag ions (in $AgNO_3$) were used to conduct a standard curve. Based on this standard curve, the concentrations of released Ag ions in the diluted nAg stock solution were determined. The proportion of Ag ions of the total Ag was about 11.6% in the diluted nAg stock solution. Meanwhile, the proportion of Ag ions was 12.2% of the total Ag with 87.8% of nAg for the diluted nAg stock solution after cloud point extraction, similar to that in the initially prepared diluted nAg stock solution before cloud point extraction, suggesting no significant dissolution of nAg during cloud point extraction.

**Detection of Reaction Oxygen Species (ROS) Production.** Generation of ROS was assessed by DCF staining. After DMSO induction for 3 d, MEL cells were cultured in 96-well plates and treated with nAg for 1, 3, 6, 12, and 24 h, followed by incubation with 10 $\mu$M DCF (Sigma-Aldrich) for 30 min at 37 °C. Thereafter, cells were subject to fluorescence analysis on a plate reader at the excitation wavelength of 488 nm and the emission wavelength of 525 nm.

**LIP Measurement by FACS.** The intracellular LIP level was determined as previously described.[79] Briefly, cells were collected and washed twice with PBS, followed by incubation with 0.5 $\mu$M CA-AM (calcein acetoxymethyl ester; Sigma-Aldrich) for 15 min at 37 °C. Thereafter, cells were washed twice with PBS and then equally divided into two parts with one treated with 100 $\mu$M DFO (Sigma-Aldrich) for 1 h at 37 °C and the other left untreated. Calcein was excited at 488 nm and measured at 525 nm with a flow cytometer (BD, FACS Calibur). Intracellular LIP value was calculated after deduction of the cellular fluorescence in DFO-treated cells by that in untreated cells.

**Statistical Analysis.** All results were presented as means ± SEM. The difference between two groups was assessed using an independent *t* test. One-way analysis of variance (ANOVA) was used to analyze the mean differences among groups compared to the control group. $P < 0.05$ was considered statistically significant.

*Conflict of Interest:* The authors declare no competing financial interest.

*Acknowledgment.* This work was supported by grants from The Chinese Academy of Sciences (KZCX2-EW-404), The National Natural Science Foundation of China (Grant Nos. 21077128, 20921063, 21177151, 21207152), and from the program, "Hundreds Talents", from the Chinese Academy of Sciences. We thank the laboratory members for their great assistance with the experiments and reagents.

*Supporting Information Available:* Details about the properties of nAg and PCR primers and additional results are provided. This material is available free of charge *via* the Internet at http://pubs.acs.org.

## REFERENCES AND NOTES

1. Sintubin, L.; Verstraete, W.; Boon, N. Biologically Produced Nanosilver: Current State and Future Perspectives. *Biotechnol. Bioeng.* **2012**, *109*, 2422–2436.
2. An Inventory of Nanotechnology-Based Consumer Products Currently on the Market. http://www.nanotechproject.org/inventories/consumer/analysis_draft/.
3. Morones, J. R.; Elechiguerra, J. L.; Camacho, A.; Holt, K.; Kouri, J. B.; Ramirez, J. T.; Yacaman, M. J. The Bactericidal Effect of Silver Nanoparticles. *Nanotechnology* **2005**, *16*, 2346–2353.
4. Shahverdi, A. R.; Fakhimi, A.; Shahverdi, H. R.; Minaian, S. Synthesis and Effect of Silver Nanoparticles on the Antibacterial Activity of Different Antibiotics against *Staphylococcus aureus* and *Escherichia coli*. *Nanomedicine* **2007**, *3*, 168–171.
5. Lu, L.; Sun, R. W.; Chen, R.; Hui, C. K.; Ho, C. M.; Luk, J. M.; Lau, G. K.; Che, C. M. Silver Nanoparticles Inhibit Hepatitis B Virus Replication. *Antiviral Ther.* **2008**, *13*, 253–262.
6. Maynard, A. D. *Nanotechnology: A Research Strategy for Addressing Risk*, Project on Emerging Nanotechnologies; Woodrow Wilson International Center for Scholars: Washington, DC, 2006; pp 1−41.
7. Chaloupka, K.; Malam, Y.; Seifalian, A. M. Nanosilver as a New Generation of Nanoproduct in Biomedical Applications. *Trends Biotechnol.* **2010**, *28*, 580–588.
8. Wijnhoven, S. W. P.; Peijnenburg, W. J. G. M.; Herberts, C. A.; Hagens, W. I.; Oomen, A. G.; Heugens, E. H. W.; Roszek, B.; Bisschops, J.; Gosens, I.; Van de Meent, D.; et al. Nano-Silver - a Review of Available Data and Knowledge Gaps in Human and Environmental Risk Assessment. *Nanotoxicology* **2009**, *3*, 109–138.
9. Christensen, F. M.; Johnston, H. J.; Stone, V.; Aitken, R. J.; Hankin, S.; Peters, S.; Aschberger, K. Nano-Silver - Feasibility and Challenges for Human Health Risk Assessment Based on Open Literature. *Nanotoxicology* **2010**, *4*, 284–295.
10. Fabrega, J.; Luoma, S. N.; Tyler, C. R.; Galloway, T. S.; Lead, J. R. Silver Nanoparticles: Behaviour and Effects in the Aquatic Environment. *Environ. Int.* **2011**, *37*, 517–531.
11. Varner, K.; Sanford, J. *State of the Science Literature Review: Everything About Nanosilver and More*; U.S. Environmental Protection Agency: Washington, DC, 2010.
12. Luoma, S. N. *Silver Nanotechnologies and the Environment: Old Problems or New Challenges*, Project on Emerging Nanotechnologies; The Pew Charitable Trusts: Washington, DC, 2008.
13. Yang, W.; Shen, C.; Ji, Q.; An, H.; Wang, J.; Liu, Q.; Zhang, Z. Food Storage Material Silver Nanoparticles Interfere with DNA Replication Fidelity and Bind with DNA. *Nanotechnology* **2009**, *20*, 085102.
14. Asharani, P. V.; Hande, M. P.; Valiyaveettil, S. Anti-Proliferative Activity of Silver Nanoparticles. *BMC Cell Biol.* **2009**, *10*, 65.
15. Hackenberg, S.; Scherzed, A.; Kessler, M.; Hummel, S.; Technau, A.; Froelich, K.; Ginzkey, C.; Koehler, C.; Hagen, R.; Kleinsasser, N. Silver Nanoparticles: Evaluation of DNA Damage, Toxicity and Functional Impairment in Human Mesenchymal Stem Cells. *Toxicol. Lett.* **2011**, *201*, 27–33.
16. AshaRani, P. V.; Low Kah Mun, G.; Hande, M. P.; Valiyaveettil, S. Cytotoxicity and Genotoxicity of Silver Nanoparticles in Human Cells. *ACS Nano* **2009**, *3*, 279–290.
17. Bar-Ilan, O.; Albrecht, R. M.; Fako, V. E.; Furgeson, D. Y. Toxicity Assessments of Multisized Gold and Silver Nanoparticles in Zebrafish Embryos. *Small* **2009**, *5*, 1897–1910.
18. Pratsinis, A.; Hervella, P.; Leroux, J. C.; Pratsinis, S. E.; Sotiriou, G. A. Toxicity of Silver Nanoparticles in Macrophages. *Small* **2013**In press.
19. Elnitski, L.; Hardison, R. Efficient and Reliable Transfection of Mouse Erythroleukemia Cells Using Cationic Lipids. *Blood Cell Mol. Dis.* **1999**, *25*, 299–304.
20. George, S.; Lin, S.; Ji, Z.; Thomas, C. R.; Li, L.; Mecklenburg, M.; Meng, H.; Wang, X.; Zhang, H.; Xia, T.; et al. Surface Defects on Plate-Shaped Silver Nanoparticles Contribute to Its Hazard Potential in a Fish Gill Cell Line and Zebrafish Embryos. *ACS Nano* **2012**, *6*, 3745–3759.
21. Zhao, C. M.; Wang, W. X. Size-Dependent Uptake of Silver Nanoparticles in *Daphnia magna*. *Environ. Sci. Technol.* **2012**, *46*, 11345–11351.
22. Liu, S.; Bhattacharya, S.; Han, A.; Suragani, R. N.; Zhao, W.; Fry, R. C.; Chen, J. J. Haem-Regulated Eif2alpha Kinase Is Necessary for Adaptive Gene Expression in Erythroid Precursors under the Stress of Iron Deficiency. *Br. J. Hamaetol.* **2008**, *143*, 129–137.
23. Hurwitz, J. The Discovery of RNA Polymerase. *J. Biol. Chem.* **2005**, *280*, 42477–42485.
24. Zhang, P.; Ma, Y.; Zhang, Z.; He, X.; Zhang, J.; Guo, Z.; Tai, R.; Zhao, Y.; Chai, Z. Biotransformation of Ceria Nanoparticles in Cucumber Plants. *ACS Nano* **2012**, *6*, 9943–9950.
25. Liu, J.; Wang, Z.; Liu, F. D.; Kane, A. B.; Hurt, R. H. Chemical Transformations of Nanosilver in Biological Environments. *ACS Nano* **2012**, *6*, 9887–9899.
26. Glover, R. D.; Miller, J. M.; Hutchison, J. E. Generation of Metal Nanoparticles from Silver and Copper Objects: Nanoparticle Dynamics on Surfaces and Potential Sources of Nanoparticles in the Environment. *ACS Nano* **2011**, *5*, 8950–8957.
27. Singh, M. P.; Atkins, T. M.; Muthuswamy, E.; Kamali, S.; Tu, C.; Louie, A. Y.; Kauzlarich, S. M. Development of Iron-Doped

Silicon Nanoparticles as Bimodal Imaging Agents. *ACS Nano* **2012**, *6*, 5596–5604.
28. Mullick Chowdhury, S.; Lalwani, G.; Zhang, K.; Yang, J. Y.; Neville, K.; Sitharaman, B. Cell Specific Cytotoxicity and Uptake of Graphene Nanoribbons. *Biomaterials* **2013**, *34*, 283–293.
29. Yu, S. J.; Chao, J. B.; Sun, J.; Yin, Y. G.; Liu, J. F.; Jiang, G. B. Quantification of the Uptake of Silver Nanoparticles and Ions to Hepg2 Cells. *Environ. Sci. Technol.* **2013**In press.
30. Sotiriou, G. A.; Pratsinis, S. E. Antibacterial Activity of Nanosilver Ions and Particles. *Environ. Sci. Technol.* **2010**, *44*, 5649–5654.
31. Wang, Z.; Chen, J.; Li, X.; Shao, J.; Peijnenburg, W. J. Aquatic Toxicity of Nanosilver Colloids to Different Trophic Organisms: Contributions of Particles and Free Silver Ion. *Environ. Toxicol. Chem.* **2012**, *31*, 2408–2413.
32. Singh, S.; Nalwa, H. S. Nanotechnology and Health Safety−Toxicity and Risk Assessments of Nanostructured Materials on Human Health. *J. Nanosci. Nanotechnol.* **2007**, *7*, 3048–3070.
33. Limbach, L. K.; Wick, P.; Manser, P.; Grass, R. N.; Bruinink, A.; Stark, W. J. Exposure of Engineered Nanoparticles to Human Lung Epithelial Cells: Influence of Chemical Composition and Catalytic Activity on Oxidative Stress. *Environ. Sci. Technol.* **2007**, *41*, 4158–4163.
34. Xia, T.; Kovochich, M.; Liong, M.; Madler, L.; Gilbert, B.; Shi, H.; Yeh, J. I.; Zink, J. I.; Nel, A. E. Comparison of the Mechanism of Toxicity of Zinc Oxide and Cerium Oxide Nanoparticles Based on Dissolution and Oxidative Stress Properties. *ACS Nano* **2008**, *2*, 2121–2134.
35. Gunawan, C.; Teoh, W. Y.; Marquis, C. P.; Amal, R. Cytotoxic Origin of Copper(II) Oxide Nanoparticles: Comparative Studies with Micron-Sized Particles, Leachate, and Metal Salts. *ACS Nano* **2011**, *5*, 7214–7225.
36. Studer, A. M.; Limbach, L. K.; Van Duc, L.; Krumeich, F.; Athanassiou, E. K.; Gerber, L. C.; Moch, H.; Stark, W. J. Nanoparticle Cytotoxicity Depends on Intracellular Solubility: Comparison of Stabilized Copper Metal and Degradable Copper Oxide Nanoparticles. *Toxicol. Lett.* **2010**, *197*, 169–174.
37. Horie, M.; Nishio, K.; Fujita, K.; Kato, H.; Nakamura, A.; Kinugasa, S.; Endoh, S.; Miyauchi, A.; Yamamoto, K.; Murayama, H.; et al. Ultrafine Nio Particles Induce Cytotoxicity in Vitro by Cellular Uptake and Subsequent Ni(II) Release. *Chem. Res. Toxicol.* **2009**, *22*, 1415–1426.
38. Park, E. J.; Yi, J.; Kim, Y.; Choi, K.; Park, K. Silver Nanoparticles Induce Cytotoxicity by a Trojan-Horse Type Mechanism. *Toxicol. In Vitro* **2010**, *24*, 872–878.
39. Cronholm, P.; Karlsson, H. L.; Hedberg, J.; Lowe, T. A.; Winnberg, L.; Elihn, K.; Wallinder, I. O.; Möller, L. Intracellular Uptake and Toxicity of Ag and CuO Nanoparticles: A Comparison between Nanoparticles and Their Corresponding Metal Ions. *Small* **2013**, *9*, 970–982.
40. Havelaar, A. C.; de Gast, I. L.; Snijders, S.; Beerens, C. E.; Mancini, G. M.; Verheijen, F. W. Characterization of a Heavy Metal Ion Transporter in the Lysosomal Membrane. *FEBS Lett.* **1998**, *436*, 223–227.
41. Bury, N. R.; Grosell, M.; Grover, A. K.; Wood, C. M. ATP-Dependent Silver Transport across the Basolateral Membrane of Rainbow Trout Gills. *Toxicol. Appl. Pharmacol.* **1999**, *159*, 1–8.
42. Chopra, I. Bacterial RNA Polymerase: A Promising Target for the Discovery of New Antimicrobial Agents. *Curr. Opin. Invest. Drugs* **2007**, *8*, 600–607.
43. Yamada, K.; Koyama, H.; Hagiwara, K.; Ueda, A.; Sasaki, Y.; Kanesashi, S. N.; Ueno, R.; Nakamura, H. K.; Kuwata, K.; Shimizu, K.; et al. Identification of a Novel Compound with Antiviral Activity against Influenza a Virus Depending on Pa Subunit of Viral RNA Polymerase. *Microbes Infect.* **2012**, *14*, 740–747.
44. Floss, H. G.; Yu, T. W. Rifamycin-Mode of Action, Resistance, and Biosynthesis. *Chem. Rev.* **2005**, *105*, 621–632.
45. Wang, Z.; Qu, G.; Su, L.; Liu, S.; Jiang, G. Evaluation of the Biological Fate and the Transport through Biological Barriers of Nanosilver in Mice. *Curr. Pharm. Des.* **2013**In press.
46. Zhang, J.; Socolovsky, M.; Gross, A. W.; Lodish, H. F. Role of Ras Signaling in Erythroid Differentiation of Mouse Fetal Liver Cells: Functional Analysis by a Flow Cytometry-Based Novel Culture System. *Blood* **2003**, *102*, 3938–3946.
47. Nair, P. M.; Park, S. Y.; Lee, S. W.; Choi, J. Differential Expression of Ribosomal Protein Gene, Gonadotrophin Releasing Hormone Gene and Balbiani Ring Protein Gene in Silver Nanoparticles Exposed *Chironomus riparius*. *Aquat. Toxicol.* **2011**, *101*, 31–37.
48. Lee, K. J.; Nallathamby, P. D.; Browning, L. M.; Osgood, C. J.; Xu, X. H. *In Vivo* Imaging of Transport and Biocompatibility of Single Silver Nanoparticles in Early Development of Zebrafish Embryos. *ACS Nano* **2007**, *1*, 133–143.
49. Welch, J. J.; Watts, J. A.; Vakoc, C. R.; Yao, Y.; Wang, H.; Hardison, R. C.; Blobel, G. A.; Chodosh, L. A.; Weiss, M. J. Global Regulation of Erythroid Gene Expression by Transcription Factor Gata-1. *Blood* **2004**, *104*, 3136–3147.
50. Griffitt, R. J.; Hyndman, K.; Denslow, N. D.; Barber, D. S. Comparison of Molecular and Histological Changes in Zebrafish Gills Exposed to Metallic Nanoparticles. *Toxicol. Sci.* **2009**, *107*, 404–415.
51. Pietroiusti, A.; Massimiani, M.; Fenoglio, I.; Colonna, M.; Valentini, F.; Palleschi, G.; Camaioni, A.; Magrini, A.; Siracusa, G.; Bergamaschi, A.; et al. Low Doses of Pristine and Oxidized Single-Wall Carbon Nanotubes Affect Mammalian Embryonic Development. *ACS Nano* **2011**, *5*, 4624–4633.
52. Yamashita, K.; Yoshioka, Y.; Higashisaka, K.; Mimura, K.; Morishita, Y.; Nozaki, M.; Yoshida, T.; Ogura, T.; Nabeshi, H.; Nagano, K.; et al. Silica and Titanium Dioxide Nanoparticles Cause Pregnancy Complications in Mice. *Nat. Nanotechnol.* **2011**, *6*, 321–328.
53. Chu, M.; Wu, Q.; Yang, H.; Yuan, R.; Hou, S.; Yang, Y.; Zou, Y.; Xu, S.; Xu, K.; Ji, A.; et al. Transfer of Quantum Dots from Pregnant Mice to Pups across the Placental Barrier. *Small* **2010**, *6*, 670–678.
54. Shimizu, M.; Tainaka, H.; Oba, T.; Mizuo, K.; Umezawa, M.; Takeda, K. Maternal Exposure to Nanoparticulate Titanium Dioxide During the Prenatal Period Alters Gene Expression Related to Brain Development in the Mouse. *Part. Fibre Toxicol.* **2009**, *6*, 20.
55. Hussain, S.; Boland, S.; Baeza-Squiban, A.; Hamel, R.; Thomassen, L. C.; Martens, J. A.; Billon-Galland, M. A.; Fleury-Feith, J.; Moisan, F.; Pairon, J. C.; et al. Oxidative Stress and Proinflammatory Effects of Carbon Black and Titanium Dioxide Nanoparticles: Role of Particle Surface Area and Internalized Amount. *Toxicology* **2009**, *260*, 142–149.
56. Lyon, T. D.; Patriarca, M.; Howatson, G.; Fleming, P. J.; Blair, P. S.; Fell, G. S. Age Dependence of Potentially Toxic Elements (Sb, Cd, Pb, Ag) in Human Liver Tissue from Paediatric Subjects. *J. Environ. Monit.* **2002**, *4*, 1034–1039.
57. Carlson, C.; Hussain, S. M.; Schrand, A. M.; Braydich-Stolle, L. K.; Hess, K. L.; Jones, R. L.; Schlager, J. J. Unique Cellular Interaction of Silver Nanoparticles: Size-Dependent Generation of Reactive Oxygen Species. *J. Phys. Chem. B* **2008**, *112*, 13608–13619.
58. Kim, S.; Choi, J. E.; Choi, J.; Chung, K. H.; Park, K.; Yi, J.; Ryu, D. Y. Oxidative Stress-Dependent Toxicity of Silver Nanoparticles in Human Hepatoma Cells. *Toxicol. In Vitro* **2009**, *23*, 1076–1084.
59. Boonstra, J.; Post, J. A. Molecular Events Associated with Reactive Oxygen Species and Cell Cycle Progression in Mammalian Cells. *Gene* **2004**, *337*, 1–13.
60. You, C.; Han, C.; Wang, X.; Zheng, Y.; Li, Q.; Hu, X.; Sun, H. The Progress of Silver Nanoparticles in the Antibacterial Mechanism, Clinical Application and Cytotoxicity. *Mol. Biol. Rep.* **2012**, *39*, 9193–9201.
61. Sotiriou, G. A.; Pratsinis, S. E. Antibacterial Activity of Nanosilver Ions and Particles. *Environ. Sci. Technol.* **2010**, *44*, 5649–5654.
62. Yamanaka, M.; Hara, K.; Kudo, J. Bactericidal Actions of a Silver Ion Solution on *Escherichia coli*, Studied by Energy-Filtering Transmission Electron Microscopy and Proteomic Analysis. *Appl. Environ. Microbiol.* **2005**, *71*, 7589–7593.

63. Bouwmeester, H.; Poortman, J.; Peters, R. J.; Wijma, E.; Kramer, E.; Makama, S.; Puspitaninganindita, K.; Marvin, H. J. P.; Peijnenburg, A. A. C. M.; Hendriksen, P. J. M. Characterization of Translocation of Silver Nanoparticles and Effects on Whole-Genome Gene Expression Using an in Vitro Intestinal Epithelium Coculture Model. *ACS Nano* **2011**, *5*, 4091–4103.
64. Liu, J. Y.; Sonshine, D. A.; Shervani, S.; Hurt, R. H. Controlled Release of Biologically Active Silver from Nanosilver Surfaces. *ACS Nano* **2010**, *4*, 6903–6913.
65. Liu, J.; Hurt, R. H. Ion Release Kinetics and Particle Persistence in Aqueous Nano-Silver Colloids. *Environ. Sci. Technol.* **2010**, *44*, 2169–2175.
66. Kawata, K.; Osawa, M.; Okabe, S. In Vitro Toxicity of Silver Nanoparticles at Noncytotoxic Doses to HepG2 Human Hepatoma Cells. *Environ. Sci. Technol.* **2009**, *43*, 6046–6051.
67. Laban, G.; Nies, L. F.; Turco, R. F.; Bickham, J. W.; Sepulveda, M. S. The Effects of Silver Nanoparticles on *Fathead minnow* (*Pimephales promelas*) Embryos. *Ecotoxicology* **2010**, *19*, 185–195.
68. Xiu, Z. M.; Zhang, Q. B.; Puppala, H. L.; Colvin, V. L.; Alvarez, P. J. Negligible Particle-Specific Antibacterial Activity of Silver Nanoparticles. *Nano Lett.* **2012**, *12*, 4271–4275.
69. Osborne, O. J.; Johnston, B. D.; Moger, J.; Balousha, M.; Lead, J. R.; Kudoh, T.; Tyler, C. R. Effects of Particle Size and Coating on Nanoscale Ag and Tio(2) Exposure in Zebrafish (*Danio rerio*) Embryos. *Nanotoxicology* **2012**In press.
70. Grosse, S.; Evje, L.; Syversen, T. Silver Nanoparticle-Induced Cytotoxicity in Rat Brain Endothelial Cell Culture. *Toxicol. In Vitro* **2013**, *27*, 305–313.
71. Levard, C.; Hotze, E. M.; Lowry, G. V.; Brown, G. E., Jr. Environmental Transformations of Silver Nanoparticles: Impact on Stability and Toxicity. *Environ. Sci. Technol.* **2012**, *46*, 6900–6914.
72. Lok, C. N.; Ho, C. M.; Chen, R.; He, Q. Y.; Yu, W. Y.; Sun, H.; Tam, P. K.; Chiu, J. F.; Che, C. M. Silver Nanoparticles: Partial Oxidation and Antibacterial Activities. *J. Biol. Inorg. Chem.* **2007**, *12*, 527–534.
73. Romanova, L.; Grand, A.; Zhang, L.; Rayner, S.; Katoku-Kikyo, N.; Kellner, S.; Kikyo, N. Critical Role of Nucleostemin in Pre-rRNA Processing. *J. Biol. Chem.* **2009**, *284*, 4968–4977.
74. Liu, S.; Suragani, R. N.; Wang, F.; Han, A.; Zhao, W.; Andrews, N. C.; Chen, J. J. The Function of Heme-Regulated Eif2alpha Kinase in Murine Iron Homeostasis and Macrophage Maturation. *J. Clin. Invest.* **2007**, *117*, 3296–3305.
75. Guang, S.; Bochner, A. F.; Burkhart, K. B.; Burton, N.; Pavelec, D. M.; Kennedy, S. Small Regulatory RNAs Inhibit RNA Polymerase II During the Elongation Phase of Transcription. *Nature* **2010**, *465*, 1097–1101.
76. Abmayr, S. M.; Yao, T.; Parmely, T.; Workman, J. L. Preparation of Nuclear and Cytoplasmic Extracts from Mammalian Cells. *Curr. Protoc. Mol. Biol.* **2006**, Chapter 12, Unit 12 11.
77. Patterson, T. A.; Lobenhofer, E. K.; Fulmer-Smentek, S. B.; Collins, P. J.; Chu, T. M.; Bao, W. J.; Fang, H.; Kawasaki, E. S.; Hager, J.; Tikhonova, I. R.; et al. Performance Comparison of One-Color and Two-Color Platforms within the Microarray Quality Control (Maqc) Project. *Nat. Biotechnol.* **2006**, *24*, 1140–1150.
78. Liu, J. F.; Chao, J. B.; Liu, R.; Tan, Z. Q.; Yin, Y. G.; Wu, Y.; Jiang, G. B. Cloud Point Extraction as an Advantageous Preconcentration Approach for Analysis of Trace Silver Nanoparticles in Environmental Waters. *Anal. Chem.* **2009**, *81*, 6496–6502.
79. Prus, E.; Fibach, E. Flow Cytometry Measurement of the Labile Iron Pool in Human Hematopoietic Cells. *Cytometry, Part A* **2008**, *73*, 22–27.